

Article

Size Distribution and Phosphate Removal Capacity of Nano Zero-Valent Iron (nZVI): Influence of pH and Ionic Strength

Dantong Lin ¹, Liming Hu ^{1,*} , Irene M. C. Lo ² and Zhigang Yu ^{2,3} 

¹ State Key Laboratory of Hydro-Science and Engineering, Department of Hydraulic Engineering, Tsinghua University, Beijing 100084, China; ldt16@mails.tsinghua.edu.cn

² Department of Civil and Environmental Engineering, The Hong Kong University of Science and Technology, Clear Water Bay, Sai Kung, Hong Kong, China; cemclo@ust.hk (I.M.C.L.); zhigang.yu@uq.net.au (Z.Y.)

³ Advanced Water Management Centre, The University of Queensland, Brisbane 4072, Australia

* Correspondence: gehu@tsinghua.edu.cn; Tel.: +86-10-62797416; Fax: +86-10-62785593

Received: 9 September 2020; Accepted: 20 October 2020; Published: 21 October 2020



Abstract: Nano zero-valent iron (nZVI) has been considered as a promising material for groundwater remediation in the past few decades. The size distribution of nZVI is one of the main factors that influences its transport capability and remediation capacity. However, studies on the size distribution of nZVI under different environmental conditions are still limited. In this study, the influence of the pH (pH = 5, 7, 9) and ionic strength (IS = 0, 15, 30, 45 mM) on the size distribution of nZVI are investigated. The dynamic light scattering (DLS) method is used to study the variation of the size distribution of nZVI aggregate with time, and batch tests are performed to evaluate the efficiency of phosphate removal. Meanwhile, the phosphate removal capacity of nZVI with different size distribution was examined. Experimental results show that under low IS and high pH conditions, nZVI aggregate exhibited a stable, narrow and one-peak size distribution. By contrast, under high IS and low pH conditions, nZVI exhibited a wide and complicated size distribution with multiple peak values. This different pattern in size distribution was further explained by the Derjaguin–Landau–Verwey–Overbeek (DLVO) theory. The phosphate removal rate of nZVI under acidic and neutral conditions is higher than 98% but is only 68% under alkaline conditions. The phosphate removal capacity is insensitive to the variation of IS since the removal rate is higher than 97% for different IS conditions. Favorable environmental conditions for colloidal stability and removal capacity of nZVI can be different, which needs comprehensive consideration in the application.

Keywords: groundwater remediation; ionic strength; pH; nano zero-valent iron (nZVI); size distribution

1. Introduction

Groundwater is the most important water resource for human beings [1]. Due to the development of industrialization and the increase in groundwater consumption, groundwater pollution has become a growing concern for people all around the world [2]. Among different types of groundwater remediation methods, an in situ remediation method has attracted the attention of researchers, due to its relatively low cost and small disturbance of the underground system [3]. In the last few decades, nanoparticles have been used as in situ remediation material in groundwater because of their minute size and high specific surface area [4]. Many sorts of nanoparticles have been studied for remediation, including nanoscale zeolites, metal oxides, carbon nanotubes, etc., among which nano zero-valent iron (nZVI) is the most extensively applied at present, due to its high activity in reaction with a variety of contaminants and low cost [5–8].

The size of nZVI is one of the main factors, which control its transport and remediation capacity. A previous study has pointed out that the transport of nZVI in groundwater is limited because of its high aggregation tendency [9]; therefore, many studies have been conducted on the aggregation process of nZVI. For example, Raychoudhury et al., (2012) tested the mean size of nZVI by a nanoparticle tracking analysis method and reported a more rapid increase in the mean size of nZVI coated with carboxymethyl cellulose with the increase in nZVI concentration [10]. Phenrat et al., (2007) studied the sedimentation curves of nZVI and pointed out that magnetic attractive forces can increase the aggregation of nZVI [11]. In previous work, the aggregation process of nZVI was usually embodied by the change in mean aggregate size with time or the optical density of the suspension [12–14], which can be seen as the average characters for aggregate with different sizes in the suspension. In the studies on the transport capacity of nZVI, the size of nZVI is one of the main parameters [15,16]. For example, in the filtration theory, which is usually used to describe the retention of nZVI [9,16,17], the collection efficiency is sensitively influenced by the size of the colloid [18,19]. The size of nZVI can increase dramatically when aggregation occurs. Duan et al. reported that aggregation of commercial nZVI happens during its transport through glass beads and studied the influence of the initial concentration [20]. However, reports on the variation of the size distribution of nZVI with time under different environmental conditions are still limited.

Since 1997, when nZVI was synthesized in the laboratory for the first time [21], researchers have proven that nZVI has high reactivity towards lots of contaminants in water, including chlorinated organic compounds, arsenic, phosphate, heavy metals and so on [22–25]. Phosphorus is one of the most common elements in the environment, while the excessive phosphorus present in groundwater can cause many environmental problems [26]. Different methods including chemical precipitation, co-precipitation and adsorption have been used to remove phosphate in water [27–29]. According to previous work, adsorption is one of the most effective methods for phosphate removal and in comparison to other adsorbents such as red mud, calcite and active carbon, nZVI is potentially an excellent adsorbent due to its high specific area and activity [30,31]. However, the environmental requirements of high colloidal stability and high removal ability can be different. Environmental conditions that are favorable for the colloid stability of nZVI may not be suitable for phosphate removal. To find an optimal environmental condition or to assess the range of application, it is meaningful to study the influence of geochemical factors, such as pH and ionic strength (IS) of the groundwater, on both of these aspects.

The objective of this study is to investigate the effects of pH and IS on the size distribution and phosphate removal capacity of nZVI in water. In this study, nZVI was synthesized in the laboratory, and the change in size distribution with time under different pH and IS conditions was tested by the dynamic light scattering (DLS) method. The Derjaguin–Landau–Verwey–Overbeek (DLVO) theory was applied to interpret how environmental factors can influence the aggregation tendency of nZVI. Batch tests were conducted to study the influence of pH and IS on the phosphate removal capacity of nZVI.

2. Materials and Methods

2.1. Synthesis of nZVI

nZVI was synthesized by a liquid-phase reduction method [21,32]. The reaction was carried out in a 250 mL 3-mouth container, with simultaneous nitrogen sparging and mechanical stirring. Sodium borohydride (NaBH_4) solution at 0.2 mol/L was drop-wise added into ferric chloride (FeCl_3) solution at 0.05 mol/L (preconditioned with N_2 sparging for deoxygenation) with a flow rate controlled at about 0.5 mL s^{-1} . After that, an additional 30 min of agitation was provided for the complete reaction between the FeCl_3 and NaBH_4 , as well as in assisting the formation of homogeneous nZVI products. Afterward, the black mixture was transferred into plastic bottles and centrifuged at 3000 rpm for 15 min. The supernatant was carefully discarded and replaced by deoxygenized deionized water (DI water,

Milli-Q, Merck, Darmstadt, Germany) to remove any unreacted residuals. The black precipitates were harvested after washing with deoxygenized DI water three times. Then, the pristine nZVI was freeze-dried for further use.

nZVI was photographed with scanning electron microscopy (SEM, JEOL JSM-6460LV, Japan Electronics Co. Ltd., Tokyo, Japan) and transmission electron microscopy (TEM, JEOL 2010 TEM, Japan Electronics Co. Ltd., Japan) to characterize its morphology. X-ray diffraction (XRD, PW-1830, Philips, Amsterdam, The Netherlands) was used to analyze the crystallinity of nZVI. Additionally, the nZVI used in the size distribution tests and batch tests was synthesized within 2 d and saved in a vacuum to avoid oxidation.

2.2. IS and pH Conditions

IS and pH are the two main environmental factors discussed in this study. The IS of the suspension was controlled as 0, 15, 30 and 45 mM by adding sodium chloride (NaCl) in DI water, according to the IS range of groundwater [33]. The pH of the suspension was controlled as 5, 7 and 9 using 0.1 M sodium hydroxide (NaOH) solution and/or hydrochloric acid (HCl) solution in DI water to reflect acidic, neutral and alkaline conditions.

2.3. Size Distribution

The size distribution of nZVI with time was recorded by a particle size analyzer (NanoBrook 90 plus zeta, Brookhaven Instruments Corporation, Holtsville, NY, USA) based on the DLS method. This method can measure the particle or aggregate size in liquid suspension by testing the fluctuation of the light intensity caused by the Brownian motion of the particles, the speed of which is related to the particle size [34]. Zeta potential of nZVI under different conditions was also measured by this equipment using the electrophoretic light scattering (ELS) method [35]. Since the range of measurement by this instrument is from 0.3 nm to 10 μm , to get a wide range of size distribution with time, 150 mg/L nZVI suspension was sonicated with ultrasonic equipment for 2 h and then filtrated by 0.45 μm filter to get a small initial size. The size distribution of the filtrate was measured every 15 min within 90 min.

2.4. Batch Tests

Batch tests were conducted to study the influence of pH and IS on nZVI's phosphate removal capacity. Firstly, 0.006 g of pristine nZVI was dispersed in 40 mL of DI water under different pH and IS conditions, as introduced in Section 2.2 (preconditioned with N_2 sparging for deoxygenation) and was sonicated for 2 h. The reaction began after 0.8 mL of 500 mg/L phosphorous (in form of monopotassium phosphate, KH_2PO_4) solution was added. The samples were shaken at 26 rpm and room temperature (23 $^\circ\text{C}$) and the adsorption kinetics was tested at 5, 10, 20, 30, 60, 90 and 120 min. For each time point, samples were prepared in triplicate and supernatants were obtained after magnetic separation. The liquid phase concentration of phosphorous was measured by inductively coupled plasma optical emission spectroscopy (ICP-OES) (Prodigy7, Teledyne Leeman Labs, Hudson, NH, USA). A flow chart of the batch test is shown in Figure 1.

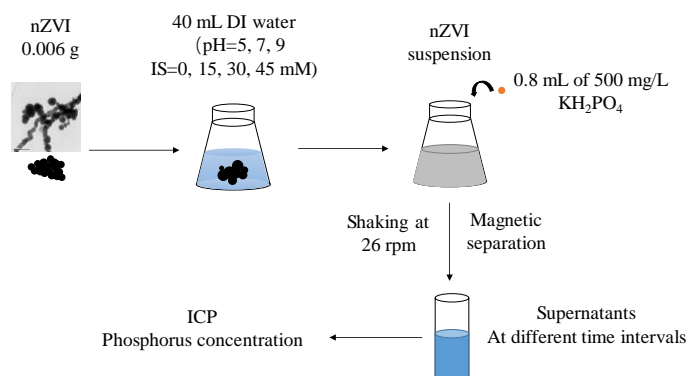


Figure 1. Flow chart of the batch test.

2.5. DLVO Theory

The colloidal stability mainly depends on the interaction between them [36]. The DLVO theory is the most commonly used theory to calculate the interaction energy between colloids [37]. The total interaction energy between two spheres E_t equals the sum of electrostatic energy E_{ES} and van der Waals attractive energy E_{vdw} , which can be given by the following equations [38,39]:

$$E_t = E_{vdw} + E_{ES} \quad (1)$$

$$E_{vdw} = -\frac{Ar}{12h\left(1 + \frac{14h}{\lambda}\right)} \quad (2)$$

$$E_{ES} = 2\pi\epsilon_0\epsilon_r h\psi_1^2 \ln(1 + e^{-\kappa h}) \quad (3)$$

where h (nm) is the distance between two spheres; $A(J)$ is the Hamaker constant of nZVI, which is usually valued as 10^{-19} ; r (nm) is the radius of spheres, which is set as the initial size of nZVI in this study; ϵ_0 ($C^2/J\cdot m$) is the permittivity of vacuum, which is 8.85×10^{-12} ; ϵ_r is the relative dielectric constant of liquid, which is 78.4 for water; ψ_1 (mV) is the surface potential of the nZVI, which is set as the tested zeta potential; κ (m^{-1}) is the inverse of Debye length, which can be expressed as:

$$\kappa = \sqrt{\frac{2N_A e^2 I}{\epsilon_r \epsilon_0 k_B T}} \quad (4)$$

where e (C) is the elementary electric charge, which is 1.6×10^{-19} ; N_A (mol^{-1}) is Avogadro's constant, which is 6.02×10^{23} ; I (mM) is the ionic strength; k_B (J/K) is Boltzmann's constant, which is 1.38×10^{-23} ; T (K) is the absolute temperature, which is 298 K.

3. Results and Discussions

3.1. Characterization of nZVI

SEM and TEM images of nZVI are shown in Figure 2a,b. Results show that the nZVI particles aggregate into a typical chain structure, which is related to the magnetic interactions between particles [40]. The size of a single particle is around 40 nm to 150 nm. The nanoscale particle size in the chain provides its high specific surface area and reactivity with contaminants.

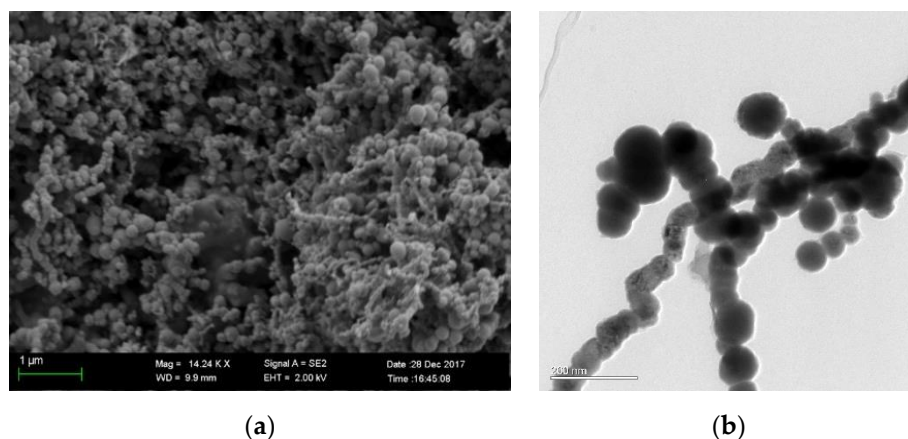


Figure 2. SEM and TEM images of nano zero-valent iron (nZVI) (a) SEM image (b) TEM image.

The XRD pattern of nZVI is shown in Figure 3. Zero valent iron (Fe^0) crystal was defined in the XRD pattern due to a peak at 2-theta around 45 [41]. Maghemite crystal is also found in nZVI because the surface of nZVI is oxidized during sample preparation, and becomes an outer shell of nZVI. The XRD results correspond to the previous report that nZVI has a core-shell structure with Fe^0 core and iron oxide shell [42]. This structure provides more sorption sites for phosphate due to the iron oxide on the surface of nZVI [41].

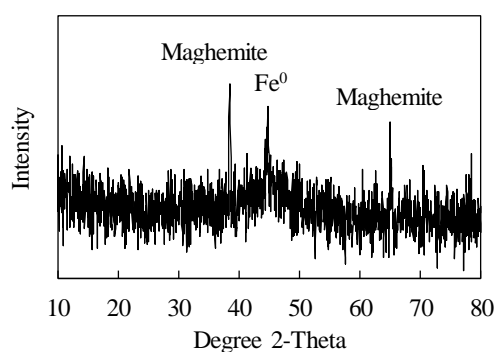


Figure 3. XRD pattern of nZVI.

3.2. Size Distribution and Mean Aggregate Size

Time-course variation of size distribution and mean size of nZVI aggregate under different pH conditions are shown in Figures 4 and 5, respectively. Under neutral and acidic conditions, the range of the size of aggregate becomes larger with an increase in mean aggregate size (Figure 4a,b). The shape of the size distribution curve becomes complicated and multimodal, usually with a small peak of less than 1000 nm and followed by the main peak of more than 1000 nm. The first peak value shows the fraction of nZVI that does not aggregate, and the second peak value shows the size of the aggregate. It is worth noticing that the range of aggregate size can change from several nanometers to several micrometers under neutral and acidic conditions. By contrast, under the alkaline condition, the size distribution was stable in 90 min, and the shape of the distribution curve was unimodal with a mean value of around 200 nm (pH = 9, Figure 4c). The mean aggregate size shown in Figure 5 implies that the aggregation tendency of nZVI under different pH is $\text{pH} = 7 > \text{pH} = 5 > \text{pH} = 9$, which is consistent with the results of sedimentation tests reported by Ibrahim et al. [12], according to the change of optical density curves.

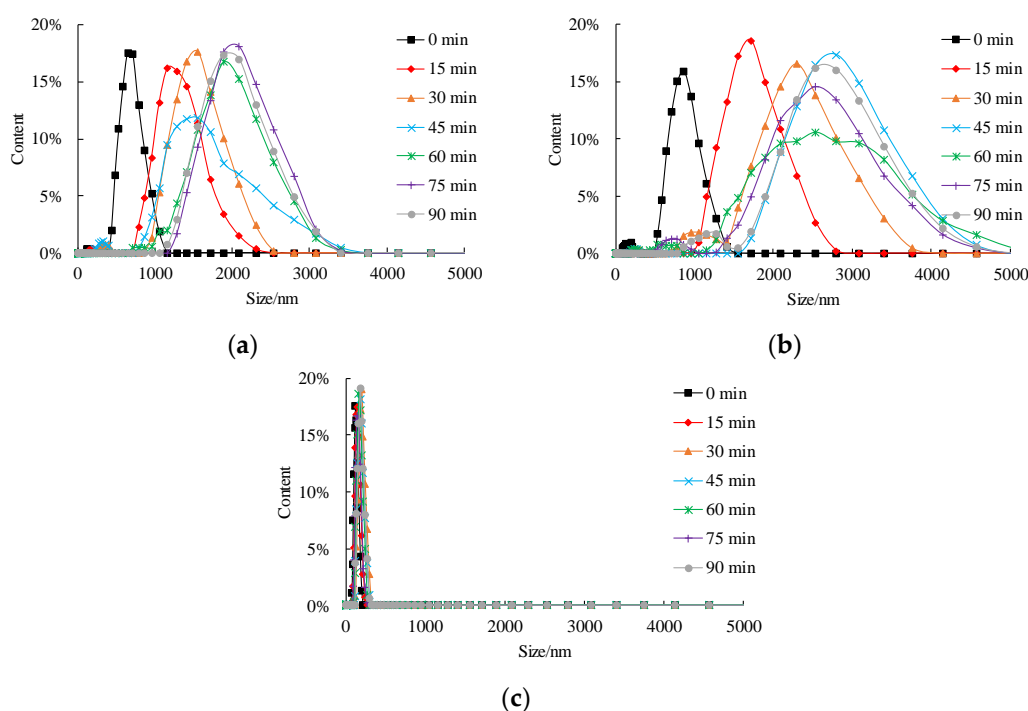


Figure 4. Influence of pH on size distribution of nZVI (a) pH = 5; (b) pH = 7; (c) pH = 9.

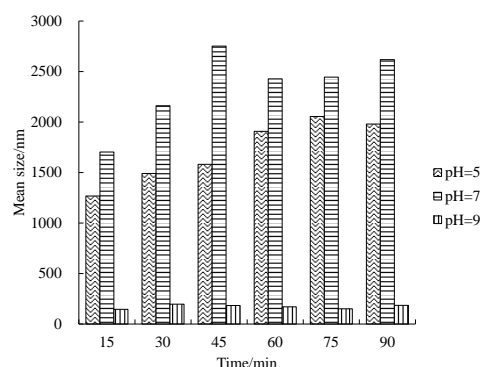


Figure 5. Mean size of nZVI with time under different pH conditions.

The influence of IS on the size distribution is shown in Figure 6, and the mean size under different IS conditions with time is shown in Figure 7. It can be observed that when IS equals zero (DI water), the size distribution of nZVI is stable; however, when IS is larger than zero, the aggregate size increases significantly. The range of size distribution is narrow when IS equals zero and when aggregation occurs under higher IS conditions, the size distribution can be complicated and have more than one peak. Furthermore, the mean size shown in Figure 7 increases with the increase in IS. Previous work reported that for bare nZVI, aggregation happens when IS is over 50 mM [12]; however, this work shows that nZVI has a high aggregate tendency even under lower IS conditions.

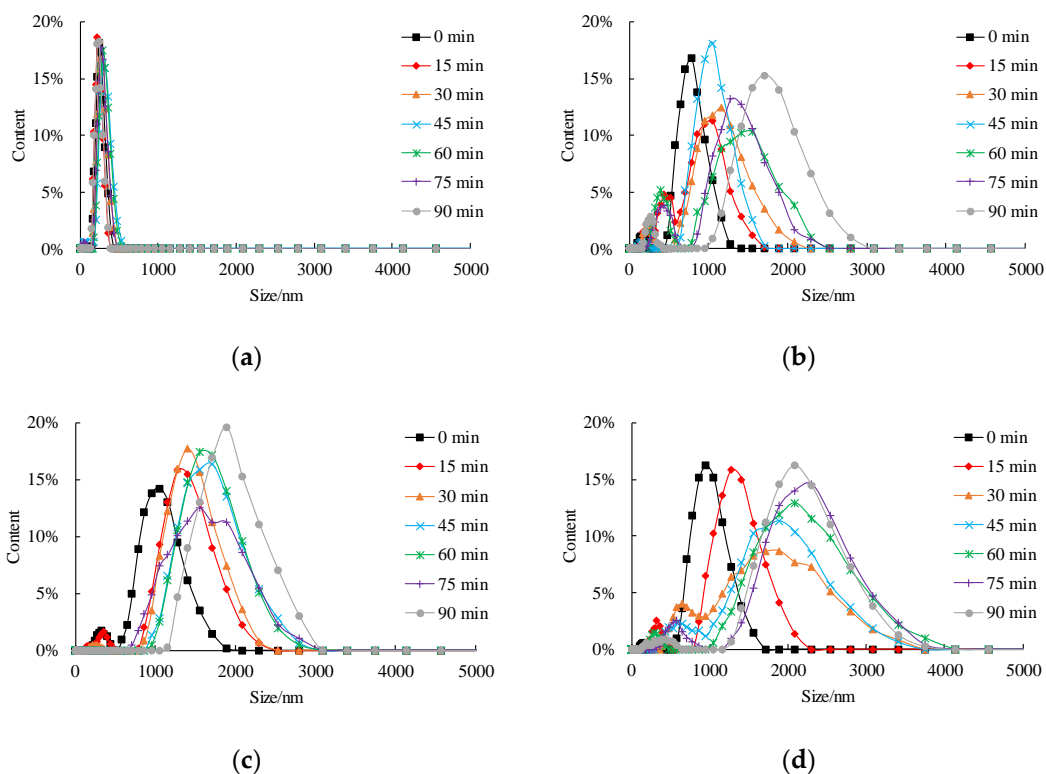


Figure 6. Influence of ionic strength (IS) on size distribution of nZVI (a) IS = 0 mM; (b) IS = 15 mM; (c) IS = 30 mM; (d) IS = 45 mM.

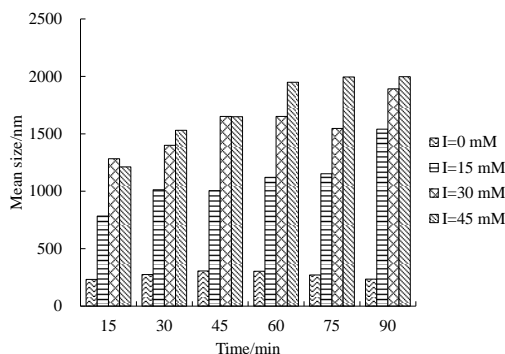


Figure 7. Mean size of nZVI with time under different IS conditions.

Single-value particle size was usually employed in previous theoretical and numerical analyses, especially for the transport model of nZVI in porous media [9,17]. This assumption can be appropriate when the size of nZVI aggregate is unchanged with time. However, according to Figures 4 and 6, the size range of nZVI is very wide (from several nanometers to several micrometers) when aggregation happens (low pH and high IS conditions). In such conditions, the single-value assumption may cause considerable deviation. The transport characteristics of nanoscale particles and microscale aggregates can be different. For example, according to filtration theory, the influence of diffusion can be more pronounced for nanoscale particles, while the influence of gravity sedimentation is more important for microscale aggregates [43]. Therefore, multiple retention mechanisms can work together in the field application of nZVI in the underground system, and the size distribution of nZVI needs to be considered in the theoretical and numerical analyses.

3.3. DLVO Calculations

The DLVO theory is usually used to analyze the stability of colloid suspension by calculating the change in interaction energy between colloids with the separation distance, which are called interaction energy curves. In this theory, the maximum point of the interaction energy curve is named the energy barrier, EB . Aggregation occurs only when the kinetic energy of the colloids exceeds EB ; therefore, the value of EB is often used to describe the stability of colloids. Figure 8 presents the interaction energy curves of nZVI under different pH and IS conditions. Figure 8a shows that the value of EB under different pH conditions meets $EB_{pH=9} > EB_{pH=5} > EB_{pH=7}$, which is consistent with the experimental observation of size distribution and mean size. The pH conditions can influence the stability of nZVI mainly by controlling the zeta potential of the aggregate and a large absolute value of zeta potential generally means good colloidal stability. The zeta potential values of nZVI for the three pH conditions are 10.8 ± 1.6 , -5.1 ± 0.6 , -22.1 ± 2.2 mV when pH values are 5, 7 and 9, respectively. Therefore, the absolute value of zeta potential can explain the observed aggregation tendency under different pH conditions.

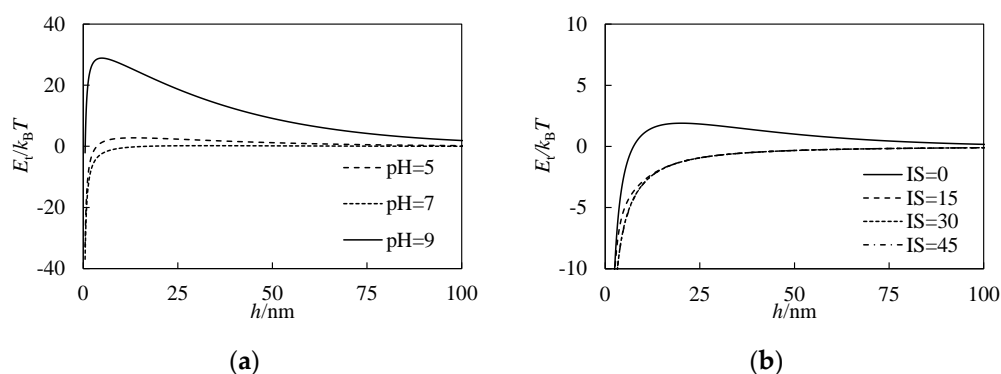


Figure 8. Interaction energy curves calculated by the Derjaguin–Landau–Verwey–Overbeek (DLVO) theory (a) under different pH conditions (b) under different IS conditions.

Figure 8b shows the interaction energy curves of nZVI under different IS conditions calculated by the DLVO theory. Results show that when IS equals 0, the EB is higher than other IS conditions. Previous work shows that IS can also influence the zeta potential [12]; however, the zeta potential of nZVI is not significantly influenced by IS (7.5 ± 1.1 , 10.4 ± 4.9 , 8.0 ± 3.4 , 10.0 ± 1.3 mV, respectively, when IS is 0, 15, 30 and 45 mM), possibly due to the relatively low IS conditions in this study. However, IS can still influence the thickness of the electric double layer, which is usually represented by Debye length, dl (m) and can be calculated as the inverse of κ in Equation (4). The increase in IS can cause a decrease in dl , which means when two colloids run into each other, the distance between them is shorter. Therefore, aggregation tendency will increase with an increase in IS of the suspension.

3.4. Phosphate Removal Capacity

The removal rate of phosphate by nZVI with time under different pH and IS conditions is shown in Figure 9. Figure 9a shows that the phosphate removal capacity of nZVI is extremely high under acidic and neutral conditions. The final removal rate was $99.4 \pm 0.3\%$ and $98.5 \pm 0.3\%$ when pH equals 5 and 7. When pH equals 9, the final removal rate decreases to $68.0 \pm 0.7\%$. The adsorption of phosphate by nZVI can be explained by the electrostatic adsorption, surface complexation and precipitation of phosphate [44]. When pH = 5, the nZVI has a positive zeta potential, which is suitable for anion sorption and the removal rate decreases under high pH conditions due to the inhibition of electrostatic adsorption [26]. Therefore, the phosphate removal capacity has an opposite trend to the pH value of the water, which is in line with the previous studies [31]. Surface complexation between the phosphate and the iron-oxide layer is another removal mechanism due to the core-shell structure of nZVI [44]. Co-precipitation of iron phosphate ($FePO_4(s)$) and ferric hydroxide ($Fe(OH)_3(s)$)

can also occur during the batch experiments [45]. Furthermore, at high pH, there could be surface passivation, which limits the reactivity of nZVI, while at low pH, the nZVI surface might have a limited oxidized layer, which leads to more active reactivity [46]. These reactions can also account for the observed results.

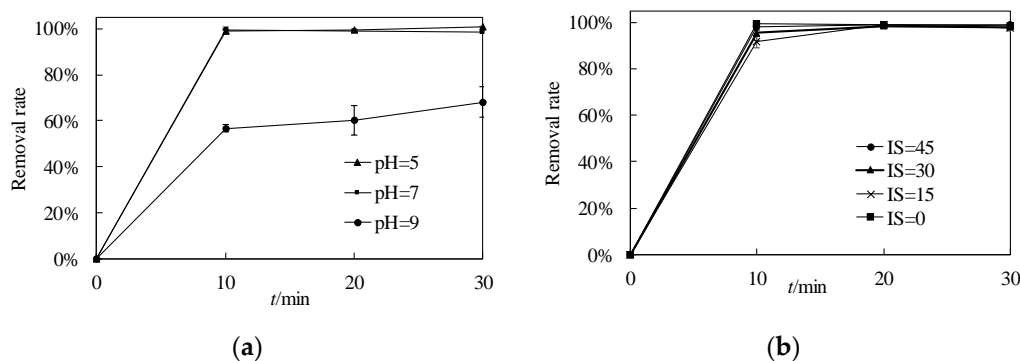


Figure 9. The removal rate of phosphate by nZVI with time (a) under different pH conditions (b) under different IS conditions.

Figure 9b exhibits the removal rate of phosphate by nZVI with time under different IS conditions. Although the colloidal stability of nZVI is influenced remarkably by IS, the impact of IS on the phosphate removal capacity is negligible, which is consistent with the previous study [26]. The final removal rate for these four IS conditions (0, 15, 30, 45 mM) was $98.5 \pm 0.3\%$, $97.3 \pm 0.1\%$, $97.9 \pm 0.5\%$, $99.1 \pm 0.6\%$, respectively, which means that nZVI maintains a good phosphate removal capacity under different IS conditions. Almeelbi and Bezbaruah also reported that IS conditions (<10 mM) do not have a significant influence on the phosphate removal capacity of nZVI [26], and according to this study, the IS range can expand to 45 mM. This phenomenon indicates that although the nZVI aggregated under these IS conditions, the surface area was still big enough for phosphate adsorption because of the small single particle size in the chain structure (as shown in Figure 2). The constant zeta potential of nZVI also coincides with the stable phosphate removal capacity under different IS conditions.

Due to the high activity of nZVI, part of nZVI can react with the hydrogen ion in water during the experiments. The dissolution percentage of nZVI at 30 min is $19.3 \pm 4.5\%$, $10.1 \pm 2.8\%$ and $0.9 \pm 0.1\%$, respectively, when pH value equals 5, 7 and 9. Results show that the dissolution rate of nZVI decreases with the increase in pH and the dissolution of nZVI is severe under acidic conditions. However, it is worth noting that under acidic conditions, although one-fifth of nZVI is dissolved in water, the removal capacity on phosphate is still high due to the positive surface potential of nZVI. Moreover, the dissolution rate of nZVI at 30 min is not significantly influenced by IS conditions ($10.1 \pm 2.8\%$, $15.6 \pm 2.6\%$, $13.9 \pm 1.3\%$ and $10.1 \pm 1.7\%$, respectively, when IS equals 0, 15, 30 and 45 mM).

According to the experiment results, the stability and phosphate removal capacity of nZVI varies with environmental conditions such as different pH levels. The stability of nZVI is better under alkaline conditions, and the removal capacity on phosphate is better under acid conditions. The geo-environment conditions should be considered in the application of nZVI. The high aggregation tendency can probably be mitigated by surface modification and the effect may vary with the choice of modifier [4,47]. Furthermore, injecting nZVI with emulsifiers may also increase its stability [48].

4. Conclusions

In this study, the size distribution and phosphate removal capacity are studied under different pH and IS conditions. The DLS method was used to measure the variation of nZVI aggregate size distribution with time and study the stability of nZVI. The DLVO theory was applied to analyze the

interaction energy between nZVI. Batch tests were conducted to study the phosphate removal capacity under different conditions. The following conclusions are drawn from the current study.

Both pH and IS have a significant influence on the size distribution of nZVI aggregate. The size distribution is stable under alkaline conditions and low IS conditions, while severe aggregation occurs under neutral/acidic conditions and high IS conditions. One of the major contributions of this study is the investigation of nZVI size distribution variation under different chemical conditions. The size of nZVI exhibits a wide distribution with the size ranging from several nanometers to several micrometers when aggregation occurs, and the size distribution curve becomes multimodal, usually with a small peak of less than 1000 nm and followed by the main peak of more than 1000 nm. The wide size distribution of nZVI shows a concern that the single-value size (usually mean aggregate size) used in many theoretical analysis models may not be suitable when aggregation occurs. The change in the aggregate size of nZVI needs to be adequately considered in numerical simulation and theoretical analysis.

The aggregation trend can be well interpreted by the DLVO theory. The height of the energy barrier (EB) in the interaction curves is used to reflect the difficulty of aggregation. Results show that the height of EB under different pH conditions meets $EB_{pH=9} > EB_{pH=5} > EB_{pH=7}$. When IS equals 0, the EB is higher than other IS conditions. The aggregation tendency predicted by the DLVO theory is consistent with the experimental observation of size distribution and mean size.

The phosphate removal capacity of nZVI is remarkably influenced by pH while the influence of IS is ignorable. The nZVI shows that the phosphate removal rate under neutral and acidic conditions is higher than 98%, while the removal rate decreases a lot under alkaline conditions to 68%. The phosphate removal capacity of nZVI remains higher than 97% under both low and high IS conditions.

In order to obtain good mobility of nZVI, an alkaline and low IS condition is needed. However, to achieve high removal capacity, the pH condition should be controlled as a weakly acidic or neutral condition. In the field application of nZVI in groundwater remediation, the different effects of IS and pH on the size distribution and removal capacity should be adequately considered. In acid or high IS environments, modification and other stabilization methods are necessary to increase the stability and transport ability of nZVI.

Author Contributions: Conceptualization, L.H. and I.M.C.L.; methodology, D.L.; investigation, D.L., L.H. and Z.Y.; writing—original draft preparation, D.L.; writing—review and editing, L.H.; supervision, L.H.; funding acquisition, L.H. and I.M.C.L. All authors have read and agreed to the published version of the manuscript.

Funding: The National Natural Science Foundation of China (51661165015) and the Research Grants Council of Hong Kong Joint Research Scheme (N_HKUST603/16) funded this research.

Conflicts of Interest: The authors declare no conflict of interest.

References

1. Koirala, S.; Yeh, J.F.; Kanae, S.; Oki, T. Explicit representation of groundwater process in a global-scale land surface model to improve the prediction of water resources. In Proceedings of the Egu General Assembly Conference, Vienna, Austria, 2–7 May 2010.
2. Beruke, A. Ground Water Resource Evaluation and Management Practices in Gilgel Abay Catchment, Tana Basin. Master's Thesis, Addis Ababa University, Addis Ababa, Ethiopia, 2012.
3. Burton, A. Hit or miss: Benefits and risks of using nanoparticles for in situ remediation. *Environ. Health Perspect.* **2009**, *117*, A552. [[CrossRef](#)] [[PubMed](#)]
4. Lefevre, E.; Bossa, N.; Wiesner, M.R.; Gunsch, C.K. A review of the environmental implications of in situ remediation by nanoscale zero valent iron (nZVI): Behavior, transport and impacts on microbial communities. *Sci. Total Environ.* **2016**, *565*, 889–901. [[CrossRef](#)]
5. Wang, H.; Cai, S.; Shan, L.; Zhuang, M.; Li, N.; Quan, G.; Yan, J. Adsorptive and reductive removal of chlorophenol from wastewater by biomass-derived mesoporous carbon-supported sulfide nanoscale zerovalent iron. *Nanomaterials* **2019**, *9*, 1786. [[CrossRef](#)] [[PubMed](#)]

6. Shi, X.D.; Ruan, W.Q.; Hu, J.W.; Fan, M.Y.; Cao, R.S.; Wei, X.H. Optimizing the removal of rhodamine b in aqueous solutions by reduced graphene oxide-supported nanoscale zerovalent iron (nzvi/rgo) using an artificial neural network-genetic algorithm (ann-ga). *Nanomaterials* **2017**, *7*, 19. [[CrossRef](#)] [[PubMed](#)]
7. Lin, D.; Zhang, Z.; Hu, L. Adsorption models of groundwater remediation by nanoscale zero valent iron. In Proceedings of the International Congress on Environmental Geotechnics, Hangzhou, China, 28 October–1 November 2018; pp. 512–520.
8. Zhang, B.; Zhu, B.-H.; Wang, X.; You, S.-B. Nanoscale Zero Valent Iron Supported by Biomass-Activated Carbon for Highly Efficient Total Chromium Removal from Electroplating Wastewater. *Water* **2019**, *12*, 89. [[CrossRef](#)]
9. Krol, M.M.; Oleniuk, A.J.; Kocur, C.M.; Sleep, B.E.; Bennett, P.; Xiong, Z.; O'Carroll, D.M. A field-validated model for in situ transport of polymer-stabilized nZVI and implications for subsurface injection. *Environ. Sci. Technol.* **2013**, *47*, 7332–7340. [[CrossRef](#)]
10. Raychoudhury, T.; Tufenkji, N.; Ghoshal, S. Aggregation and deposition kinetics of carboxymethyl cellulose-modified zero-valent iron nanoparticles in porous media. *Water Res.* **2012**, *46*, 1735–1744. [[CrossRef](#)]
11. Phenrat, T.; Saleh, N.; Sirk, K.; Tilton, R.D.; Lowry, G.V. Aggregation and sedimentation of aqueous nanoscale zerovalent iron dispersions. *Environ. Sci. Technol.* **2007**, *41*, 284–290. [[CrossRef](#)]
12. Ibrahim, H.M.; Awad, M.; Al-Farraj, A.S.; Al-Turki, A.M. Stability and dynamic aggregation of bare and stabilized zero-valent iron nanoparticles under variable solution chemistry. *Nanomaterials* **2020**, *10*, 192. [[CrossRef](#)]
13. Busch, J.; Meissner, T.; Potthoff, A.; Oswald, S.E. Investigations on mobility of carbon colloid supported nanoscale zero-valent iron (nZVI) in a column experiment and a laboratory 2D-aquifer test system. *Environ. Sci. Pollut. Res. Int.* **2014**, *21*, 10908–10916. [[CrossRef](#)]
14. Yin, K.; Lo, I.M.; Dong, H.; Rao, P.; Mak, M.S. Lab-scale simulation of the fate and transport of nano zero-valent iron in subsurface environments: Aggregation, sedimentation, and contaminant desorption. *J. Hazard. Mater.* **2012**, *227–228*, 118–125. [[CrossRef](#)]
15. Kocur, C.M.; O'Carroll, D.M.; Sleep, B.E. Impact of nZVI stability on mobility in porous media. *J. Contam. Hydrol.* **2013**, *145*, 17–25. [[CrossRef](#)] [[PubMed](#)]
16. Yu, Z.; Hu, L.; Lo, I.M.C. Transport of the arsenic (As)-loaded nano zero-valent iron in groundwater-saturated sand columns: Roles of surface modification and As loading. *Chemosphere* **2019**, *216*, 428–436. [[CrossRef](#)]
17. Raychoudhury, T.; Surasani, V.K. Implication of surface modified NZVI particle retention in the porous media: Assessment with the help of 1-D transport model. *J. Earth Syst. Sci.* **2017**, *126*, 56. [[CrossRef](#)]
18. Chatterjee, J.; Gupta, S.K. An agglomeration-based model for colloid filtration. *Environ. Sci. Technol.* **2009**, *43*, 3694–3699. [[CrossRef](#)] [[PubMed](#)]
19. Tufenkji, N.; Elimelech, M. Correlation equation for predicting single-collector efficiency in physicochemical filtration in saturated porous media. *Environ. Sci. Technol.* **2004**, *38*, 529–536. [[CrossRef](#)]
20. Duan, R.; Dong, Y.; Zhang, Q. Characteristics of Aggregate Size Distribution of Nanoscale Zero-Valent Iron in Aqueous Suspensions and Its Effect on Transport Process in Porous Media. *Water* **2018**, *10*, 670. [[CrossRef](#)]
21. Wang, C.B.; Zhang, W.X. Synthesizing nanoscale iron particles for rapid and complete dechlorination of TCE and PCBs. *Environ. Sci. Technol.* **1997**, *31*, 2154–2156. [[CrossRef](#)]
22. Zhu, H.; Jia, Y.; Wu, X.; Wang, H. Removal of arsenic from water by supported nano zero-valent iron on activated carbon. *J. Hazard. Mater.* **2009**, *172*, 1591–1596. [[CrossRef](#)]
23. Kaifas, D.; Malleret, L.; Kumar, N.; Fetimi, W.; Claeys-Bruno, M.; Sergent, M.; Doumenq, P. Assessment of potential positive effects of nZVI surface modification and concentration levels on TCE dechlorination in the presence of competing strong oxidants, using an experimental design. *Sci. Total Environ.* **2014**, *481*, 335–342. [[CrossRef](#)]
24. Wang, Y.; Fang, Z.; Kang, Y.; Tsang, E.P. Immobilization and phytotoxicity of chromium in contaminated soil remediated by CMC-stabilized nZVI. *J. Hazard. Mater.* **2014**, *275*, 230–237. [[CrossRef](#)]
25. Wen, Z.; Zhang, Y.; Dai, C. Removal of phosphate from aqueous solution using nanoscale zerovalent iron (nZVI). *Colloids Surf. A Physicochem. Eng. Asp.* **2014**, *457*, 433–440. [[CrossRef](#)]
26. Almeelbi, T.; Bezbaruah, A. Aqueous phosphate removal using nanoscale zero-valent iron. *J. Nanopart. Res.* **2012**, *14*, 900. [[CrossRef](#)]
27. Hauduc, H.; Takacs, I.; Smith, S.; Szabo, A.; Murthy, S.; Daigger, G.T.; Sperandio, M. A dynamic physicochemical model for chemical phosphorus removal. *Water Res.* **2015**, *73*, 157–170. [[CrossRef](#)]

28. Singh, A.K.; Singh, K.P. Optimization of phosphate removal from aqueous solution using activated carbon supported zero-valent iron nanoparticles: Application of RSM approach. *Appl. Water Sci.* **2018**, *8*, 226. [[CrossRef](#)]
29. Sleiman, N.; Deluchat, V.; Wazne, M.; Mallet, M.; Courtin-Nomade, A.; Kazpard, V.; Baudu, M. Phosphate removal from aqueous solution using ZVI/sand bed reactor: Behavior and mechanism. *Water Res.* **2016**, *99*, 56–65. [[CrossRef](#)]
30. Zhang, Q.; Liu, H.; Chen, T.; Chen, D.; Li, M.; Chen, C. The Synthesis of NZVI and Its Application to the Removal of Phosphate from Aqueous Solutions. *Water Air Soil Pollut.* **2017**, *228*, 321. [[CrossRef](#)]
31. Ding, A. Phosphate removal from aqueous solutions by nanoscale zero-valent iron. *Environ. Technol.* **2013**, *34*, 2663–2669.
32. Sun, Y.P.; Li, X.Q.; Cao, J.; Zhang, W.X.; Wang, H.P. Characterization of zero-valent iron nanoparticles. *Adv. Colloid Interface Sci.* **2006**, *120*, 47–56. [[CrossRef](#)]
33. Heo, J.-H.; Lee, D.-H.; Koh, D.-C.; Chang, H.-W. The effect of ionic strength and hardness of trichloroethylene-contaminated synthetic groundwater on remediation using granular activated carbon. *J. Geosci.* **2007**, *11*, 229–239. [[CrossRef](#)]
34. Sats, A.; Mootse, H.; Pajumaegi, S.; Pisponen, A.; Tatar, V.; Poikalainen, V. Estimation of particle size distribution in bovine colostrum whey by dynamic light scattering (dls) method. *Agron. Res.* **2014**, *12*, 801–806.
35. Varenne, F.; Botton, J.; Merlet, C.; Vachon, J.-J.; Geiger, S.; Infante, I.C.; Chehimi, M.M.; Vauthier, C. Standardization and validation of a protocol of zeta potential measurements by electrophoretic light scattering for nanomaterial characterization. *Colloids Surf. A Physicochem. Eng. Asp.* **2015**, *486*, 218–231. [[CrossRef](#)]
36. Sun, P.; Shijirbaatar, A.; Fang, J.; Owens, G.; Lin, D.; Zhang, K. Distinguishable Transport Behavior of Zinc Oxide Nanoparticles in Silica Sand and Soil Columns. *Sci. Total Environ.* **2015**, *505*, 189–198. [[CrossRef](#)]
37. Phenrat, T.; Saleh, N.; Sirk, K.; Kim, H.-J.; Tilton, R.D.; Lowry, G.V. Stabilization of aqueous nanoscale zerovalent iron dispersions by anionic polyelectrolytes: Adsorbed anionic polyelectrolyte layer properties and their effect on aggregation and sedimentation. *J. Nanopart. Res.* **2007**, *10*, 795–814. [[CrossRef](#)]
38. De Vicente, J.; Delgado, A.V.; Plaza, R.C.; Duran, J.D.G.; Gonzalez-Caballero, F. Stability of cobalt ferrite colloidal particles. Effect of pH and applied magnetic fields. *Langmuir* **2000**, *16*, 7954–7961. [[CrossRef](#)]
39. Hogg, R.; Healy, T.W.; Fuerstenau, D.W. Mutual Coagulation of Colloidal Dispersions. *Trans. Faraday Soc.* **1966**, *62*, 1638–1651. [[CrossRef](#)]
40. Rončević, S.; Nemet, I.; Ferri, T.Z.; Matković-Čalogović, D. Characterization of nZVI nanoparticles functionalized by EDTA and dipicolinic acid: A comparative study of metal ion removal from aqueous solutions. *RSC Adv.* **2019**, *9*, 31043–31051. [[CrossRef](#)]
41. Maamoun, I.; Eljamal, O.; Khalil, A.M.E.; Sugihara, Y.; Matsunaga, N. Phosphate Removal Through Nano-Zero-Valent Iron Permeable Reactive Barrier; Column Experiment and Reactive Solute Transport Modeling. *Transp. Porous Media* **2018**, *125*, 395–412. [[CrossRef](#)]
42. Yan, W.; Herzing, A.A.; Kiely, C.J.; Zhang, W.X. Nanoscale zero-valent iron (nZVI): Aspects of the core-shell structure and reactions with inorganic species in water. *J. Contam. Hydrol.* **2010**, *118*, 96–104. [[CrossRef](#)]
43. Molnar, I.L.; Johnson, W.P.; Gerhard, J.L.; Willson, C.S.; O'Carroll, D.M. Predicting colloid transport through saturated porous media: A critical review. *Water Resour. Res.* **2015**, *51*, 6804–6845. [[CrossRef](#)]
44. Nagoya, S.; Nakamichi, S.; Kawase, Y. Mechanisms of phosphate removal from aqueous solution by zero-valent iron: A novel kinetic model for electrostatic adsorption, surface complexation and precipitation of phosphate under oxic conditions. *Sep. Purif. Technol.* **2019**, *218*, 120–129. [[CrossRef](#)]
45. Caravelli, A.H.; Contreras, E.M.; Zaritzky, N.E. Phosphorous removal in batch systems using ferric chloride in the presence of activated sludges. *J. Hazard. Mater.* **2010**, *177*, 199–208. [[CrossRef](#)] [[PubMed](#)]
46. Song, H.; Carraway, E. Reduction of chlorinated ethanes by nano-sized zero-valent iron. *Environ. Sci. Technol.* **2005**, *39*, 6237–6245. [[CrossRef](#)] [[PubMed](#)]
47. Dong, H.; Lo, I.M.C. Transport of Surface-Modified Nano Zero-Valent Iron (SM-NZVI) in Saturated Porous Media: Effects of Surface Stabilizer Type, Subsurface Geochemistry, and Contaminant Loading. *Water Air Soil Pollut.* **2014**, *225*, 2107. [[CrossRef](#)]

48. Long, T.; Andrewramburg, C. Encapsulation of nzvi particles using a gum arabic stabilized oil-in-water emulsion. *J. Hazard. Mater.* **2011**, *189*, 801–808. [[CrossRef](#)]

Publisher’s Note: MDPI stays neutral with regard to jurisdictional claims in published maps and institutional affiliations.



© 2020 by the authors. Licensee MDPI, Basel, Switzerland. This article is an open access article distributed under the terms and conditions of the Creative Commons Attribution (CC BY) license (<http://creativecommons.org/licenses/by/4.0/>).